The Journal of Chemical Physics

RESEARCH ARTICLE | AUGUST 29 2025

Analyzing the internal interface in localized high-concentration electrolytes

Special Collection: Chemical physics of ionic transport in solvents, polymers, and near interfaces

Anne Hockmann ; Monika Schönhoff ; Diddo Diddens

J. Chem. Phys. 163, 084719 (2025)
https://doi.org/10.1063/5.0285201

The Journal of Chemical Physics ARTICLE pubs.aip.org/aip/jcp

Analyzing the internal interface in localized high-concentration electrolytes

Cite as: J. Chem. Phys. 163, 084719 (2025); doi: 10.1063/5.0285201
Submitted: 13 June 2025 • Accepted: 6 August 2025 •
Published Online: 29 August 2025

Anne Hockmann,[1,2] Monika Schönhoff,[1] and Diddo Diddens[1,3,a)]

AFFILIATIONS

[1] Institute of Physical Chemistry, University of Münster, Corrensstraße 28/30, 48149 Münster, Germany
[2] International Graduate School Battery Chemistry, Characterization, Analysis, Recycling, and Application (BACCARA), University of Münster, Corrensstraße 40, 48149 Münster, Germany
[3] Helmholtz Institute Münster, IMD-4, Forschungszentrum Jülich GmbH, Corrensstraße 48, 48149 Münster, Germany

Note: This paper is part of the Special Topic, Chemical Physics of Ionic Transport in Solvents, Polymers, and Near Interfaces.
[a)]**Author to whom correspondence should be addressed:** d.diddens@fz-juelich.de

ABSTRACT

We present molecular dynamics simulations on localized high-concentration electrolytes (LHCE) based on the conducting salt lithium bis(fluorosulfonyl)imide (LiFSI) or lithium bis(trifluoromethanesulfonyl)imide dissolved in the solvent 1,2-dimethoxyethane and diluted to two different degrees with the diluent 1,1,2,2-tetrafluoroethyl-2,2,3,3-tetrafluoropropyl ether. Due to the immiscibility of the conducting salt phase (salt + solvent) and the diluent phase, LHCEs feature a complex microstructure of two phases forming an internal interface. In this study, we not only investigate the lithium coordination structure in the conducting salt phase but also the size and composition of its interface to the diluent phase by Voronoi tessellations. Furthermore, we investigate the influence on the ion transport by evaluating Onsager coefficients. We show that an LHCE containing the surface-active anion $TFSI^-$ creates an anion-rich internal interface, leading to enhanced ion dissociation and anticorrelated ion movement. On the other hand, the smaller FSI^- anion with a more localized charge distribution and less amphiphilic character shows no enrichment at the internal interface, but rather a depletion. By increasing LiFSI concentration, we even observe a solvent-rich internal interface due to a large and branched Li–anion network. Furthermore, the less diffuse interface and enlarged Li–anion network lead to lower ion–ion anticorrelations and a stronger convective flux of the conducting salt phase, which is compensated by a flux of the diluent phase, especially in the higher concentrated LiFSI based LHCE.

INTRODUCTION

While the worldwide energy demand is increasing, current state-of-the-art lithium ion batteries (LIB) reach their fundamental limits such that alternative post-LIB technologies gain rising attention.[1] Especially lithium metal batteries (LMB) offer promising features, such as a low redox potential and an ultrahigh theoretical capacity. However, introducing a lithium metal anode leads to severe safety issues; therefore, different types of electrolyte, liquid and solid, are currently being investigated to overcome these challenges. Promising liquid electrolytes, e.g., are high-concentration electrolyte (HCE) and localized high-concentration electrolytes (LHCE).[2–5] In both cases, a high amount of conducting salt is dissolved in an organic solvent to decrease the ratio of free and reactive solvent molecules and thereby improve the stability against the anode. Furthermore, due to the large proportion of anions in the first coordination shell of Li^+, the solid electrolyte interphase is predominantly formed from anions, resulting in the inhibition of both, lithium dendrite growth and dissolution of the aluminum current collector, as well as achieving a good galvanostatic cycling stability.[3,6]

To obtain an LHCE, a non-coordinating low viscosity solvent, the diluent, is additionally included. Resulting from the immiscibility of the diluent with the conducting salt phase, the unique characteristic of an LHCE is a heterogeneous microstructure consisting of a conducting salt phase, as in the HCE, and an additional diluent phase. Thereby, the viscosity is reduced and the wettability improved, without affecting the lithium coordination structure. This mitigates the shortcomings, but retains the benefits of an HCE.[3,4,7]

Despite this complex microstructure of LHCEs, most of the research to date has focused on screening potential constituents and compositions to improve performance, physical, and electrochemical properties.[8–11] Apart from this, theoretical studies mainly dealt with the impact of dilution on the first lithium coordination shell, changes in HOMO/LUMO levels, and the related reactions and processes at the electrode|electrolyte interface.[12] As an example for coordination analysis, Wu *et al.* showed that the diluent does not participate in the solvation of Li^+, but leads to a lower binding energy of Li^+ and its ligands, i.e., the solvent (DMC, dimethyl carbonate) and the anion [FSI^-, bis(fluorosulfonyl)imide]. Moreover, they reported a slightly increased coordination number (CN) of O_{DMC} and a reduced CN of O_{FSI} upon dilution. These changes resulted in a reduced reduction stability of the anion and increased lithium self-diffusion.[13] A few studies investigate the impact of the diluent on the overall electrolyte microstructure and lithium ion transport in the bulk. For example, some describe Li^+ ion transport as an ion hopping mechanism, which is disrupted due to the addition of the diluent phase.[14,15] Using SAXS, Raman spectroscopy, and molecular dynamics (MD) simulations, Efaw *et al.* investigated the complex LHCE microstructure and developed a ternary phase diagram to describe and predict the solvation structure in a LiFSI–DME–TFEO [lithium bis(fluorosulfonyl)imide, dimethoxyethane, and tris(2,2,2-trifluoroethyl)orthoformate] LHCE. They proposed a micelle-like structure with a higher conducting salt concentration at the center of the salt cluster, while the solvent, which is enriched at the interface with the diluent phase, is acting as a surfactant between the two phases.[16] In a previous publication,[17] we experimentally investigated the interplay between conducting salt phase and diluent phase and proposed that the composition of the conducting salt|TTE interface depends on the anion structure. While a DME-enriched interface is reasonable for the LiFSI/DME-based LHCE, we demonstrated that in a LiTFSI [lithium bis(trifluoromethanesulfonyl)imide]/DME-based LHCE, the ratio of free and dynamic anions increases, suggesting their enrichment at the interface due to a more beneficial interaction of $TFSI^-$ with the diluent, in this case 1,1,2,2-tetrafluoroethyl-2,2,3,3-tetrafluoropropyl ether (TTE).

In the present work, we evaluate MD simulations of three different electrolyte formulations based on LiFSI or LiTFSI as the conducting salt, DME as the solvent, and TTE to dilute the HCE, in analogy to our previous experimental study.[17] We show that depending on composition and the employed anion, either anions or solvent molecules are enriched at the conducting salt|TTE interface, offering a way to deliberately tune these LHCEs. In particular, we employed the basic Voronoi analysis and domain analysis[18] implemented in the software Travis[19,20] to elucidate the size and composition of the conducting salt|TTE interface. This tool offers the possibility to define neighboring molecules without any additional criterium such as a cutoff distance, which makes it particularly useful in this case since we aim to describe a very fuzzy interface rather than a well-defined coordination shell. Moreover, the Voronoi analysis provides not only contact partners but also contact areas. Therefore, unprecedented additional information on the size of the conducting salt|TTE interface is obtained. Furthermore, we analyze the influence of dilution on the local lithium coordination environment, the Li–anion network, the internal interface formed between conducting salt and diluent phase, and use this information on the solvation structure to explain the observed differences in ion–ion correlations affecting the overall conductivity. We confirm our previous experimental results and provide a straightforward method to study the conducting salt|TTE interface and its influence on the coordination structure and dynamics.

SIMULATION DETAILS

Molecular dynamics (MD) simulations were performed using the software package GROMACS (version 2019.3)[21] with Canongia Lopes and Pádua (CL & P) force field[22] for the ions and Optimized Potentials for Liquid Simulations All Atom (OPLS-AA) force field[23] for the solvent and diluent. In case of the latter, LigParGen has been used to create the initial topologies.[24] The ionic charges were scaled by a factor of 0.8 as reported elsewhere in the literature to account for polarization effects.[25,26] We simulated an increasing degree of dilution with TTE for three different electrolyte formulations, referred to as LiTFSI(1.8), LiFSI(1.8), and LiFSI(1.2) based on the employed conducting salt and the molar fraction of the solvent DME. The electrolyte compositions were chosen in accordance to our previous paper; the details are shown in Table S1. Three-dimensional periodic cubic simulation boxes were generated by means of PACKMOL[27] containing around 800 molecules in total. The final box volumes are listed in Table S1. The initialization was followed by two relaxation runs of 10 ns each under NPT conditions. The first one was performed at 700 K and the second one at the target temperature of 299.65 K. After that, the system was equilibrated for 100 ns and the final production run was an NVT simulation for 1 μs. To ensure the simulations are consistent with the experimental systems, we compared obtained densities and diffusion coefficients with our previously published experimental values; see Figs. S1 and S2. In view of the limitations of non-polarizable force fields, deviations between the absolute values occur; however, the relative trends of the experimental data are well-reflected. The simulation trajectories were analyzed with scripts supported by the Python library MDAnalysis[28,29] and Travis.[18–20]

RESULTS AND DISCUSSION

In this paper, we investigate the influence of diluting an HCE with the non-coordinating diluent, TTE, for three different systems: one based on LiTFSI dissolved in DME with a conducting salt to solvent molar ratio of 1:1.8, which is close to its saturation limit, referred to as LiTFSI(1.8); a stoichiometrically equal HCE based on LiFSI, referred to as LiFSI(1.8); and finally, a higher concentrated LiFSI-based HCE with a conducting salt/solvent ratio of 1:1.2, LiFSI(1.2). The latter ratio is again close to the saturation limit. For all systems, we compare the HCE to two dilution levels with diluent/conducting salt molar ratios: n(TTE) = 1 and n(TTE) = 2.

Lithium coordination environment

To analyze how dilution influences the lithium coordination structure, we evaluate radial distribution functions (RDF), $g(r)$. Figure 1 presents RDFs of oxygen atoms of all species around Li^+ for the LiTFSI-based electrolytes [HCE in Fig. 1(a), LHCEs in Figs. 1(b) and 1(c)]. In addition, since a coordination between F–Li is stated in the literature for some diluents,[30–32] the distribution of the

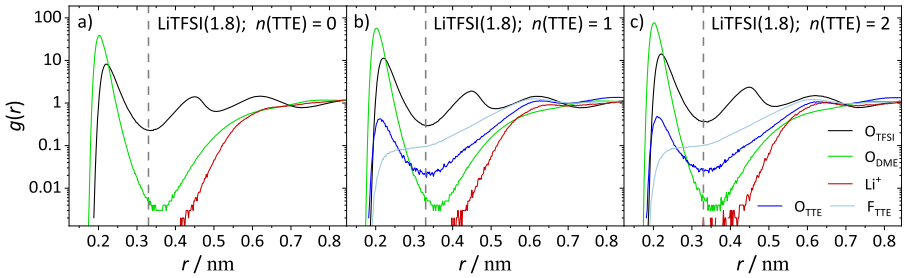

FIG. 1. $g(r)$ of O_{DME} (green), O_{anion} (black), O_{TTE} (dark blue), F_{TTE} (light blue), and Li^+ (red) around Li^+ for the LiTFSI-based electrolytes: (a) HCE, (b) n(TTE) = 1, and (c) n(TTE) = 2. The dashed gray line signifies the cutoff distance of 0.33 nm for the first lithium solvation shell.

fluorine atoms of the diluent is shown too. RDFs of the LiFSI-based electrolytes are shown in Fig. S3 and exhibit similar trends.

First of all, Fig. 1 shows that the coordination environment is largely unaltered upon dilution: while the RDFs of O_{anion}–Li and O_{DME}–Li show a clear peak with a maximum at around ~0.22 nm for all degrees of dilution, the peaks of O_{TTE} and F_{TTE} for the first lithium solvation shell are rather small. Thus, the Li^+ cation is almost exclusively coordinated by anions and DME, independent of the degree of dilution, suggesting that two phases, the conducting salt and diluent phase, are formed as intended for LHCE and in accordance to the literature.[30]

For a more in-depth investigation, we calculated coordination numbers (CN) by defining a cutoff radius of 0.33 nm for the first coordination shell of Li^+ (vertical gray lines shown in Figs. 1 and S3) and integrating the peak areas. The results are shown in Figs. 2 and S4 for all compositions. As already mentioned, the contribution of the diluent in the solvation of Li^+ is very small, resulting in an average CN for O_{TTE} between 0.01 and 0.04, as shown in Fig. S4. Slightly higher values are obtained for the shoulder observed for the F_{TTE}–Li coordination (0.1–0.2). However, this is rather due to the higher abundance of F-atoms in the TTE molecule than a strongly preferential coordination. Figure 2(a) depicts the minor impact of F_{TTE} on the total CN for all systems and degrees of dilution (compare open and filled red diamonds: O-atoms only vs O- and F-atoms). Therefore, in the following discussion, we neglect the Li–F coordination and focus on the main contributors to the lithium solvation.

Next to the already mentioned total CN of O-atoms (sum of CN of O_{anion}, O_{DME}, and O_{TTE}), CN_{O_tot}, and O- and F-atoms (sum of CN of O_{anion}, O_{DME}, O_{TTE}, and F_{TTE}), Fig. 2(a) shows the

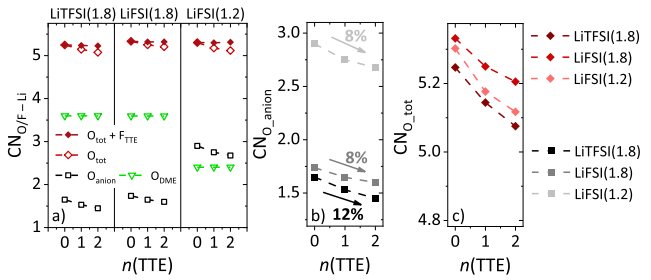

FIG. 2. Lithium coordination numbers CN from RDF. (a) Average CN of O_{DME} (green), O_{anion} (black), O_{tot} (O_{anion} + O_{DME} + O_{TTE}; open red diamonds), and O_{tot} + F_{TTE} (O_{anion} + O_{DME} + O_{TTE} + F_{TTE}; filled red diamonds) as a function of dilution for LiTFSI(1.8), LiFSI(1.8), and LiFSI(1.2) HCE (from left to right). (b) CN(O_{anion}) and (c) CN(O_{tot}) in dependence on the degree of dilution for all systems.

CN of the two main ligands, anion and solvent for all systems, and degrees of dilution. First, a very constant CN(O_{DME}), green triangles, is observed for all systems, which equals the total O_{DME} available: CN(O_{DME}) = 3.6 for the two stoichiometrically identical (L)HCEs LiTFSI(1.8), on the left, and LiFSI(1.8), in the middle, while it is CN(O_{DME}) = 2.4 for the higher concentrated LiFSI(1.2) system on the right-hand side. Thus, due to their strong bidentate coordination, all DME molecules coordinate Li^+ and no free solvent molecules are present. This is expected and reported for a similar system in a previous publication over a range of conducting salt concentrations from low to high conducting salt concentrations.[33] Moreover, we observe a total CN of around 5.3 oxygen atoms for all electrolyte formulations, which is in accordance to the literature reporting coordination numbers between four to six oxygens.[34–39] An optimal coordination by six oxygen atoms is most probably not achieved due to the high conducting salt concentration, heterogeneous coordination environment (DME and anion), and the resulting inefficient packing of the conducting salt phase. Regarding the average CN of O_{anion}, Fig. 2(a) shows CN of around 1.7 for LiTFSI(1.8) and LiFSI(1.8), while it is CN(O_{anion}) = 2.8 in the LiFSI(1.2) system. Thus, in the lower concentrated systems, the most frequent Li^+ coordination partner is DME, while the coordination environment in the higher concentrated LiFSI(1.2) system is slightly anion dominated.

Taking a closer look on the just discussed anion coordination, the close-up in Fig. 2(b) shows a decrease upon dilution in all three systems. The addition and growth of the diluent phase interrupts the Li–anion coordination, leading to a decreasing CN. Interestingly; such a break up is not observed for the Li–DME coordination. The strong bidentate coordination by DME is not influenced by the addition of a TTE phase.

Moreover, this decrease in CN(O_{anion}) is a little stronger in the LiTFSI-based LHCE (12% decrease for the stronger diluted system compared to the HCE) in comparison with both LiFSI-based electrolytes (decrease of 8%). While the precise value of these percentages might in general depend on the employed force field, a recent study[16] suggests that CN(O_{DME}) and CN(O_{anion}) are rather insensitive to the employed charge scaling factor (see Sec. II) for an HCE with a similar composition as the conducting salt phase in our systems. Similar findings are reported elsewhere in the literature.[40,41] Therefore, we expect that the relevant trends discussed above and in the following would essentially remain preserved if other force field parameters were used. This is further confirmed by Raman spectra that we analyzed in an earlier publication[17] on these systems, where we observed an increasing share of free TFSI anions upon dilution, while this was not the case in the LiFSI-based systems.

Furthermore, the stronger decrease in $CN(O_{anion})$ upon dilution of the LiTFSI(1.8) system leads to a more pronounced decrease in CN_{O_tot} upon dilution [see Fig. 2(c)] in comparison with the stoichiometrically equivalent LiFSI-based electrolyte composition, LiFSI(1.8). Furthermore, we note a general trend for the absolute values of CN_{O_tot} for all degrees of dilution according to: LiFSI(1.8) > LiFSI(1.2) > LiTFSI(1.8). In the electrolyte with the more bulky anion $TFSI^-$, Li^+ is most strongly undercoordinated due to sterical hindrance and less effective packing in the conducting salt phase compared to the stoichiometrically identical LiFSI(1.8) system. Here, CN_{O_tot} is the highest, since compared to the higher concentrated LiFSI(1.2) system more DME molecules are part of the coordination shell, again leading to less sterical hindrance and a more feasible packing. Since the lithium coordination by anions undergoes the most significant changes upon dilution, we will take a more detailed look on this coordination in the next two sections.

Mono vs bidentate coordination by the anion

Since the investigated systems are all highly concentrated and the average $Li–O_{anion}$ CN is above one (1.7 or even 2.8), the distribution of mono- vs bidentate coordination is analyzed in this section. While a bidentate coordination is probably sterically less favored in such a highly concentrated conducting salt phase, a large fraction of monodentate coordination would imply an average coordination to more than one Li^+ per anion, resulting in an extended Li–anion network.

To answer this question, we evaluated the RDF of the nitrogen atom of the anion around Li^+, as shown in Fig. 3(a). In the case of $TFSI^-$ (black line), the RDF shows two close peaks with maxima at 0.38 and 0.45 nm. These peaks can be attributed to bidentate and monodentate coordinated $TFSI^-$ anions, respectively.[42] For both LiFSI-based systems, a third peak at an even smaller distance, 0.23 nm, is observed, corresponding to a direct coordination of Li^+ by the N-atom of FSI^-.[43] The CN for the different types of coordination are compared in Fig. 3(b). First, as already noticed from Fig. 3(a), a direct Li–N coordination is observed for the FSI^- anion (middle and right section), which is more pronounced in the higher concentrated LiFSI(1.2) system on the right side. However, with CNs between 0.10 and 0.17, the contribution of this type of coordination is rather small and constant with dilution.

However, not only direct N–Li coordination is more frequent in the FSI-based systems but also a bidentate coordination. While the monodentate coordination clearly dominates in the TFSI-based system (left-hand side), the monodentate coordination more or less equals the bidentate coordination in both systems containing FSI^- anions. This finding is in accordance with the previous results, again implying a stronger sterical hindrance in the system with the bulkier $TFSI^-$ anion and a more compact solvation shell in the LiFSI-based electrolytes with the smaller anion featuring a more localized charge distribution.

Upon dilution, the weaker monodentate coordination decreases more strongly in all systems indicating that monodentate coordination can be interrupted more easily by the introduction of a TTE phase. Thus, the higher share of easily disrupted monodentate coordination compared to bidentate coordination in the TFSI-based LHCE is probably also the reason why the coordination by O_{anion} decreases more strongly in general; see Fig. 2(b).

Regarding the highest concentrated LiFSI(1.2) system, Fig. 3(b) shows an average coordination number of ~1 for both bidentate and monodentate coordinations. Thus, Li^+ is on average coordinated by two anions: one coordinating in a monodentate and one in a bidentate fashion. Since the stochiometric ratio between anion and cation is 1:1, this finding implies that some anions coordinate more than one lithium cation, leading to a larger Li–anion network. Such a network would result in a certain Li–Li distance observed as a peak in the Li–Li RDF. As expected and seen from Fig. 3(c), a clear Li–Li peak is observed in the highest concentrated LiFSI(1.2) system with a maximum of around 0.6 nm, which is in accordance to the literature.[44] In comparison, the Li–Li peak is less pronounced in the LiTFSI(1.8) and LiFSI(1.8) systems due to the lower conducting salt concentration. Interestingly, the Li–Li peak in the LiFSI(1.2) system increases upon dilution [see Fig. 3(d)], although TTE interrupts the conducting salt phase and the average $CN(O_{anion})$ decreases [see Fig. 2(b)]. To elucidate this counterintuitive finding, we take a closer look at the distribution of the number of lithium cations coordinating to one given anion (anion-centered Li–anion CNs), as illustrated in Fig. 4.

The histograms shown in Figs. 4(a) and 4(b) illustrate the probability of the CN by lithium ions for a given anion in dependence on the amount of diluent (anion-centered Li–anion CNs) in the stoichiometrically equal LiTFSI(1.8) and LiFSI(1.8) systems,

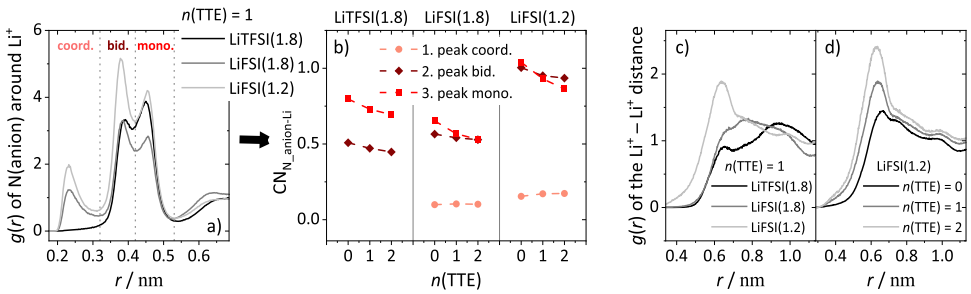

FIG. 3. (a) N_{anion}–Li RDF [LiTFSI(1.8) black, LiFSI(1.8) dark-gray, LiFSI(1.2) light-gray] with n(TTE) = 1 revealing direct N–Li coordination (first peak), bidentate (second peak), and monodentate (third peak) O–Li coordination. (b) Distribution of direct (light-red circles), bi- (dark-red diamond), and monodentate (red squares) coordination for the dilution of LiTFSI(1.8), LiFSI(1.8), and LiFSI(1.2) HCE (from left to right). (c) Li–Li RDF for LiTFSI(1.8) black, LiFSI(1.8) dark-gray, LiFSI(1.2) light-gray at n(TTE) = 1 and (d) Li–Li RDF for dilution of LiFSI(1.2) (increasing dilution from black to light-gray).

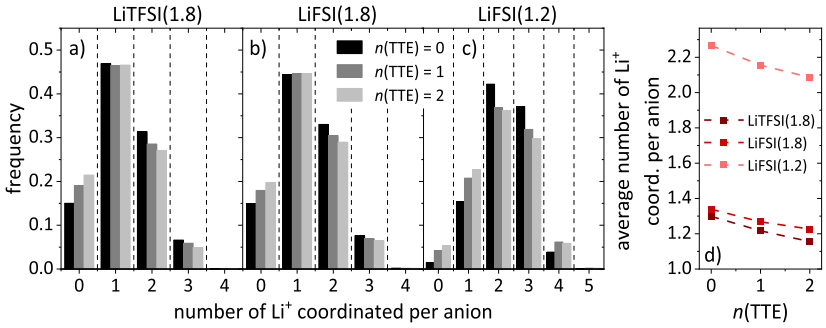

FIG. 4. Distribution of anion-centered Li–anion CNs with increasing dilution (black to light-gray) (a) LiTFSI(1.8), (b) LiFSI(1.8), (c) LiFSI(1.2). (d) Average anion-centered Li–anion CNs in dependence on the degree of dilution for all systems.

respectively. These systems show very similar distributions. The most frequent coordination with around 45% is one Li^+ per anion, followed by a coordination by two Li^+ with about 30%. Furthermore, a significant number of free anions (~15%) is observed, and a small amount of 3Li–anion coordination environments (~5%), but a negligible amount of four Li^+ per anion. Thus, just one neighboring Li^+ cation is the dominant coordination in these systems; however, a significant amount of linearly bridging anions (CN = 2) is present too. Moreover, upon dilution, the probability for high coordination numbers (2 or 3) decreases, while the number of free anions increases. The Li–anion network gets interrupted by the TTE phase, leading to weaker coordinated or even non-coordinated anions at the conducting salt|TTE interface, as discussed in more detail in the following.

The histogram of the higher concentrated LiFSI(1.2) system shown in Fig. 4(c) reveals that CN = 1 is less frequent (20%), while two (~38%) and three (~32%) are the most frequent coordination numbers. Moreover, a notable amount of 4Li–anion coordination is present (~5%), while the number of free anions is significantly smaller (~5%) compared to the systems with a higher amount of DME. Therefore, in LiFSI(1.2), bridging anions clearly dominate and the bridging is not only linear (involving 2 Li^+) but also branched (3 Li^+), implying a large and possibly more complex Li–anion network. This also explains why a clear Li–Li peak in $g(r)$ is observed [see Fig. 3(c)].

In agreement with the systems discussed in Figs. 4(a) and 4(b), lower coordination numbers of zero and one increase upon dilution, while higher CN of two and three decrease. However, the amount of four neighboring Li^+ increases too (4%–6%). This implies that in this case, dilution promotes an increase in both weakly and highly coordinated anions. Presumably, this exceptional distribution of CNs corresponds to a formation of two anion coordination environments: anions at the center of the conducting salt phase phase coordinating multiple cations and anions located at the conducting salt|TTE interface interacting with the diluent and coordinating a maximum of one Li^+. Moreover, referring back to Fig. 3(d), the increase in Li–Li ordering can be explained by this increase in highly coordinated anions.

Size of Li-anion network

The actual size of these Li–anion networks is illustrated in Fig. 5. In Fig. 5(a) to (c), snapshots are shown for the very diluted state [n(TTE) = 2] of the LiTFSI(1.8), LiFSI(1.8), and LiFSI(1.2) LHCE, respectively, presenting the lithium cations (red) and all

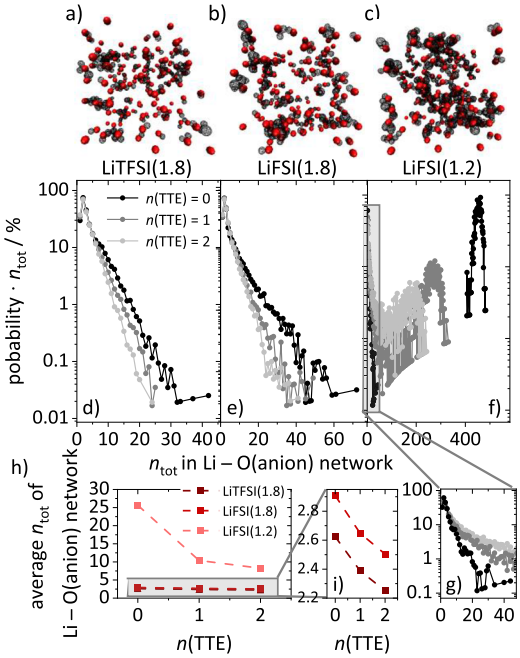

FIG. 5. Li–anion network size. Snapshots of the Li–anion network at a high degree of dilution [n(TTE) = 2] for (a) LiTFSI(1.8), (b) LiFSI(1.8), and (c) LiFSI(1.2). Li^+ is indicated by red, and atoms of the anions within a distance of 0.33 nm of Li^+ are indicated by black. Probability of an ion being involved in a cluster of a certain size for the different dilutional states (from black to light-gray) of (d) LiTFSI(1.8), (e) LiFSI(1.8), and (f) LiFSI(1.2). (g) Section of panel (f) focusing on the small clusters. (h) Average cluster size in dependence on n(TTE). (i) Section of panel (h).

atoms of the anions in a distance of 0.33 nm to a cation (black surface). The same snapshots are also included in the SI at a larger scale [see Figs. S5(a)–S5(c)]. In accordance with the results in Sec. III B, the largest connected black surfaces are observed for LiFSI(1.2) LHCE, confirming the high Li–FSI CN and large Li–FSI networks. However, some smaller clusters exist too. The Li–FSI networks are significantly smaller in the lower concentrated LiFSI(1.8) LHCE [Fig. 5(b)] and even slightly smaller in the LHCE containing TFSI anions [Fig. 5(a)].

By counting the connected Li–anion bonds, a size distribution of Li–anion networks can be determined. Multiplying this size distribution with the number of ions involved in the particular network

($n_{cluster}$) provides the probability that an ion belongs to a Li–anion network of a given size, as shown in Figs. 5(d)–5(g). As expected, the LiTFSI(1.8) based electrolyte, Fig. 5(d), exhibits the smallest clusters (<40 ions). Here, ion pairs and very small cluster are most frequent. However, due to the presence of a few larger clusters, the total average cluster size is ~2.4, as shown in Figs. 5(h) and 5(i). Ion pairs as the dominant species might seem counterintuitive for a highly concentrated electrolyte; however, so far, we did not include DME in our evaluation, for which we already showed that it is the dominant coordination partner of Li^+ in the LiTFSI(1.8) and LiFSI(1.8) electrolytes [see Fig. 2(a)]. However, since DME cannot extend the salt network due to its bidentate coordination, it might terminate the Li–anion network, resulting in a large fraction of small networks. Furthermore, Figs. 5(h) and 5(i) show that the total network size decreases upon dilution due to the interruption of the salt network by the addition of a diluent phase.

Comparable results are obtained for the stoichiometrically equivalent FSI^- based system shown in Fig. 5(e). Again, ion pairs and small clusters dominate, however, in comparison with the LiTFSI-based system, even larger clusters of up to 70 ions are observed. This results in a somewhat higher average network size of ~2.6 [cf. ~2.4 in the LiTFSI based (L)HCEs] and can be explained by the smaller size of the anion, leading to a more efficient packing of the conducting salt phase and thus, larger Li–anion networks. However, a comparable decrease in average cluster size upon dilution is observed.

The highly concentrated LiFSI(1.2) electrolytes shown in Figs. 5(f) and 5(g) exhibit the largest connected Li–anion coordination, by far, corresponding to large clusters percolating the entire simulation box [close to 500 ions in the HCE and up to 350 ions in the LHCE, although it should be noted that the distribution in Fig. 5(g) is affected by the size of the simulation box]. This is consistent with the higher $Li–O_{anion}$ CN and more pronounced bridging of the anion. In accordance with the previously discussed systems, free ions and ion pairs are still most frequent at least in the diluted electrolytes [see Fig. 5(f) light and dark gray line]. However, as already mentioned, we observe a pronounced probability of an ion being part of very large salt networks involving >150 ions. Moreover, in contrast to the lower concentrated systems shown in Figs. 5(d) and 5(e), the highest concentrated LiFSI(1.2) system in Fig. 5(f) does not show a monotonously decreasing shape of the size distribution. Rather, this simulation box consists of several free ions and ion pairs on one side and one large Li–anion network on the other side, with the latter comprising most of the ions in the system. This leads to an average cluster size of ~25 ions in HCE and ~10 ions in LHCEs. Thus, the LiFSI(1.2) system exhibits the most significant decrease in average cluster size upon dilution. In addition, the heatmaps shown in Fig. S6 demonstrate that the salt clusters are predominantly neutral ($N_{cation} = N_{anion}$) or have a low net charge in relation to the total number of ions for all investigated systems.

As already mentioned, we have not yet included DME in our analysis of the conducting salt networks; however, it likely affects the overall morphology of the conducting salt phase as well. To account for its contribution, we used the domain analysis implemented in Travis,[18] which is based on calculating Voronoi cells and evaluating their contacts to other cells. Defining cation, anion, and DME as one domain, we can calculate how many individual conducting salt domains are formed. By averaging over all time steps of the final production run in each simulation, we obtain a probability of percolation, i.e., the probability of observing only one continuous conducting salt phase. This probability is 99.4% even in the system with the smallest Li–anion network [LiTFSI(1.8) with n(TTE) = 2]. Similarly, by defining all TTE molecules as one domain, we can also calculate the probability of percolation for the TTE phase. Here, we obtain a probability of 99.1%. Thus, a bicontinuous system is formed.

Conducting salt|TTE interface size and composition

Snapshots of the conducting salt phases are shown in Figs. 6(a)–6(c) and S5(d)–S5(f) (larger scale). Again, Li^+ is displayed in red and anions in black, but now DME (green) molecules within a distance of 0.33 nm of Li^+ are additionally depicted. A comparison with Figs. 5(a)–5(c) reveals once again the visually evident major contribution of DME in the coordination of Li^+. Figures 6(a)–6(c) show a continuous conducting salt phase with a very fuzzy interface toward the diluent phase (TTE molecules not shown). The LHCE microstructure of two immiscible phases is very special and affects not only ion transport but also other important parameters such as electrochemical properties and battery performance.[45] Therefore, we investigated the formation of the conducting salt|TTE interface in more detail by taking a closer look at its size and composition shown in Figs. 6(d)–6(f). The already mentioned domain analysis provides

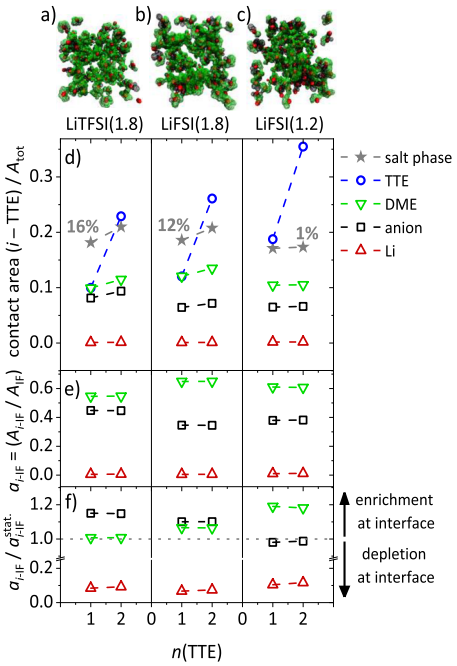

FIG. 6. Snapshots of the conducting salt phase at a high degree of dilution [n(TTE) = 2] for (a) LiTFSI(1.8), (b) LiFSI(1.8), (c) LiFSI(1.2). Li^+ in red; anion (black) and DME (green) in a distance of 0.33 nm of Li^+. The influence of further dilution on the contact area between the different species [TTE: blue circles, DME: green triangles, anion: black squares, salt phase (sum of Li^+, anion, and DME): gray stars] and TTE: normalized to (d) A_{tot}, (e) A_{IF}, and (f) $a_{i-IF}^{stat.}$, for the systems LiTFSI(1.8), LiFSI(1.8), and LiFSI(1.2), from left to right.

the average contact area of Voronoi cells of different species, A_{i-j}.[18] Furthermore, the average surface area of each species is given as A_i. From this, the total intrinsic area, A_{tot}, can be calculated as the sum over the surfaces of all molecules/ions in the system, partitioned into contributions for each species i; see the following equation:

$$A_{tot} = A_{Li} + A_{Anion} + A_{DME} + A_{TTE} = \sum_i A_i. \quad (1)$$

Figure 6(d) presents the changes in the contribution of the contact areas (i – TTE) to the total intrinsic area upon dilution for the LHCEs LiTFSI(1.8), LiFSI(1.8), and LiFSI(1.2) (left to right). First, as expected, the fraction of TTE–TTE contacts (blue circles) increases with an increasing amount of diluent in all simulations. It is also apparent that the fraction of Li^+–TTE contacts is negligible. The small and Pearson hard cations are strongly coordinated by anions and DME and do not interact with TTE molecules. Thus, the interface between conducting salt and TTE phase is formed almost exclusively by anions and solvent molecules.

Figure 6(d) shows that the fraction of DME–TTE contact area, $A_{DME-TTE}$, is larger compared to the anion–TTE contact area, $A_{anion-TTE}$, in all systems. Thus, the DME molecule is the dominant species at the conducting salt|TTE interface, which was expected since the organic solvent can interact with the unpolar diluent. Moreover, no Li–DME coordination needs to be broken [see Fig. 2(a)], as DME can interact with TTE via its protons while coordinating lithium in a bidentate fashion through its oxygen atoms. However, the difference between the fractions of anion–TTE and DME–TTE contacts is significantly smaller in the LiTFSI(1.8)-based system (left-hand side). On the one hand, this can be explained by a size effect: The bulkier $TFSI^-$ creates more anion–TTE interface when interacting with TTE. On the other hand, a preferential interaction between $TFSI^-$ and TTE is probably also more likely compared to FSI^-. As shown by density functional theory calculations,[46] the charge delocalization in $TFSI^-$ is more pronounced, resulting in a weaker electrostatic potential near the terminal CF_3-groups when compared to the fluorine atoms of FSI^-. Consequently, one would expect a more amphiphilic character, leading to a more beneficial interaction with the nonpolar diluent. This explanation matches the smaller lithium coordination number of $TFSI^-$ and the smaller Li–anion networks obtained for the LiTFSI-based LHCE [see Fig. 5(i)]. Moreover, Fig. 6(d) shows that the total conducting salt|TTE interface,

$$A_{IF} = A_{Li-TTE} + A_{Anion-TTE} + A_{DME-TTE} = \sum_{i \neq TTE} A_{i-TTE}, \quad (2)$$

increases more strongly upon dilution in the LiTFSI-based LHCE (16%, gray stars) compared to the stoichiometrically equal LiFSI-based LHCE (12%), implying that the formation of the interface is more favored in the LHCE containing $TFSI^-$ anions.

A_{IF} is slightly smaller in the higher concentrated LiFSI(1.2) LHCE and, remarkably, almost independent on the degree of dilution [increase of 1%; in Fig. 6(d), see the gray stars on the right-hand side]. Thus, upon dilution, the TTE–TTE contacts increase strongly (blue circles) without enlarging the conducting salt|TTE interface (gray stars). This is consistent with the previous results on the high lithium coordination number of the anions and large and branched Li–anion networks in this system: due to the small molar fraction of DME, which can easily form the interface toward the TTE phase, the formation of conducting salt|TTE interface is often accompanied by the disruption of the Li–anion network leading to a more pronounced undercoordination of Li^+, which is unfavorable.

Figure 6(e) presents the different contributions to the conducting salt phase–TTE contact area normalized to the total conducting salt|TTE interface; see the following equation:

$$a_{i-IF} = \frac{A_{i-TTE}}{A_{IF}} = \frac{A_{i-TTE}}{A_{Li-TTE} + A_{Anion-TTE} + A_{DME-TTE}} = \frac{A_{i-TTE}}{\sum_{i \neq TTE} A_{i-TTE}}. \quad (3)$$

As expected, the fraction of the different constituents is the same as in Fig. 6(d); however, it is striking that this distribution is constant upon dilution. Thus, the composition of the conducting salt|TTE interface is independent of its size.

To elucidate a preferred occurrence of a given species at the interface toward the TTE phase, we define $a_{i-IF}^{stat.}$ as the statistical distribution of the components of the conducting salt phase at the conducting salt |TTE interface based on the molecular surfaces (A_i) and amounts (n_i) in the conducting salt phase; see the following equation:

$$a_{i-IF}^{stat.} = \frac{n_i \cdot A_i}{n_{Anion} \cdot A_{Anion} + n_{DME} \cdot A_{DME} + n_{Li} \cdot A_{Li}} = \frac{n_i \cdot A_i}{\sum_{i \neq TTE} n_i \cdot A_i}. \quad (4)$$

Next, we normalized the actual fraction of each component at the interface, a_{i-IF}, to $a_{i-IF}^{stat.}$ to probe deviations from the statistical distribution. Thereby, the different size and concentration of each species is accounted for. Values larger than one correspond to an enrichment of a species at the conducting salt|TTE interface, while values below one reflect depletion. The obtained values are shown in Fig. 6(f).

First, a clear depletion of Li^+ is observed. As already mentioned, an interaction between the nonpolar diluent and the small Li^+ cation is very unfavorable, so that Li^+ hardly participates in the formation of the interface toward the diluent. Therefore, in LiFSI(1.8) LHCE (see the middle panel), the contribution of DME and FSI^- is slightly above a statistical distribution to compensate for the depletion of Li^+ at the interface. This particle distribution at the internal interface is also illustrated in Scheme 1(b).

In the higher concentrated LiFSI(1.2) LHCE, only the fraction of DME is clearly above one and the contribution of FSI^- is slightly below one (see the right panel). Once again, this points out that the anion is less likely to form the interface due to the high share of bridging anions in this system. Therefore, a clear enrichment of DME at the interface is observed, and the composition of the conducting salt|TTE interface differs from the bulk composition: While DME is predominantly creating the interface toward the diluent phase, lithium cations coordinated by FSI^- anions dominate the core of the conducting salt phase [also see Scheme 1(c)].

Interestingly, in contrast to the LiFSI-based LHCEs, an enrichment of TFSI anions at the conducting salt|TTE interface is found in the LiTFSI-based LHCE, while DME basically shows an ideal behavior regarding its presence at the interface [see the left panel of

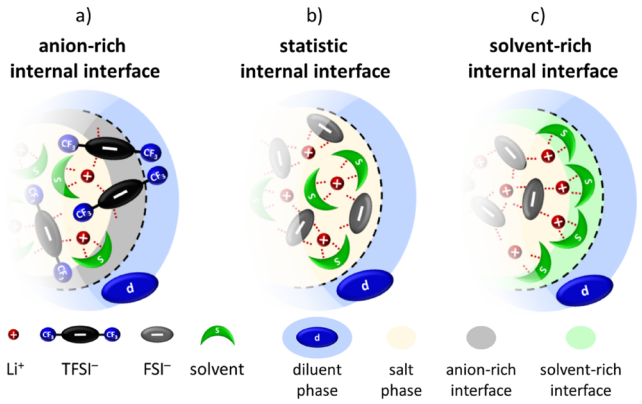

SCHEME 1. Schematic illustration of the composition at the internal conducting salt|TTE interface for (a) LiTFSI(1.8), (b) LiFSI(1.8), and (c) LiFSI(1.2). The diluent phase is depicted in blue, conducting salt phase in yellow, and an enrichment of one species at the interface is marked in gray (anions) or green (solvent).

Fig. 6(f) and Scheme 1(a)]. This result clearly shows that the higher share of $TFSI^-$ anion at the interface is not only a size effect, but rather due to the more beneficial interaction with TTE, as discussed above. Thus, $TFSI^-$ is more surface active compared to FSI^-. These findings corroborate the conclusions that were previously drawn from an extensive experimental investigation of these LHCEs.[17]

Impact on the dynamics

To gain information on how ion transport is influenced by the discussed structural differences, ion correlations, relevant for the migration of ions in an electric field, can be calculated from equilibrium simulations through the framework of Onsager transport coefficients within the linear response regime. In a binary electrolyte, three ion–ion correlations are relevant: cation–cation (σ_{++}), anion–anion (σ_{--}), and cation–anion correlations (σ_{+-}); see Eqs. (S1)–(S3). Furthermore, the expressions for the like-ion correlations can be split into a self (σ_i^{self}) and distinct part (σ_i^{d}); see Eqs. (S4) and (S5). Using these definitions, the Nernst–Einstein conductivities [σ_{ion_NE}, see Eq. (S6)] can be calculated, which describe the ionic conductivity with neglect of ion correlations. Furthermore, ionic conductivities (σ_{ion}) and the inverse Haven ratio (H_R^{-1}), also known as ionicity and given by the ratio $\sigma_{ion}/\sigma_{ion\_NE}$, can be determined, see Eqs. (S7) and (S8). In accordance with experimental inverse Haven ratios,[17] the values decrease for all simulations upon dilution, as shown in Fig. S7. This indicates that the addition of a diluent accelerates the self-diffusion of the ions due to the reduced viscosity, while charge transport is less influenced. As TTE does not interfere with the Li^+ coordination shell, the local Li^+ transport mechanisms may not change too much upon dilution, while on the other hand, the transport of larger clusters of the conducting salt phase in the very fluid diluent contributed largely to the diffusion coefficients, which enter σ_{ion_NE}. As migrating clusters of the conducting salt phase are largely uncharged, this leads to smaller changes in ionic conductivity compared to the diffusivities. Furthermore, we note that the H_R^{-1} values calculated from MD simulations overestimate the experimental values (see Fig. S7). Presumably, this is due to the limitations of approximating polarization interactions by scaling ion charges in nonpolarizable force fields.[47] However, the trends obtained from simulations resemble the real system quite well (cf. Figs. S2 and S7), thus a qualitative investigation of ion correlations is reasonable.

Figure 7 shows the cation–anion correlation and the distinct like-ion correlations normalized to σ_{ion}. These three quantities generally follow the trend, $\sigma_{--}^{d} \approx \sigma_{++}^{d} < \sigma_{+-}$. Moreover, in the HCE simulations [n(TTE) = 0], all three Onsager coefficients are negative, reflecting anticorrelated motion of the ionic species. This is in accordance to the literature and can be explained by the volume conservation constraint, which was demonstrated to be valid for incompressible high-concentration electrolytes.[48–50] We note that strictly speaking, MD simulations are usually performed in the center-of-mass frame; however, it was recently shown that ion correlations are largely governed by the incompressibility constraint, which is compatible with volume conservation.[51]

With the addition of a diluent, all Onsager coefficients increase. The cation–anion correlation even becomes positive upon dilution in all systems. This indicates a net movement of Li^+ and anions in the same direction. Due to the high conducting salt concentration, the anion is a crucial part of the Li^+ coordination environment (see Fig. 2). Thus, cations and anions are direct neighbors and a correlated movement in the same direction is likely to occur. However, due to incompressibility, more remote regions of the electrolyte have to move in an anticorrelated manner to compensate for this locally correlated motion, which was recently shown by a distance-dependent analysis of the Onsager coefficients in ionic liquids.[51] For a HCE, this compensating flux (volume conservation) is largely established by other ions, leading to smaller average values for the ion correlations. In the LHCE systems, however, the diluent phase contributes to volume conservation as well. This allows a correlated convective flux of the conducting salt phase, compensated by the flux of the diluent phase, leading to larger average ion correlations and thus less anticorrelated motion. This is also reflected by the like-ion correlations: In the case of the LiTFSI(1.8) and LiFSI(1.8) system (left and middle section), both like-ion correlations also increase upon dilution but remain negative. Since like-ions are less likely to be direct neighbors in the cation–anion network, the local positive correlation is weaker and their net movement remains anticorrelated due to the overall compensating flux. Furthermore, our results

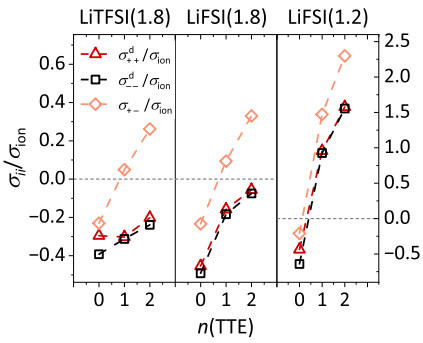

FIG. 7. Onsager coefficients normalized to σ_{ion} in dependence on the degree of dilution for the systems LiTFSI(1.8), LiFSI(1.8), and LiFSI(1.2), from left to right. σ_{++}^{d}: red triangles, σ_{--}^{d}: black squares, and σ_{+-}: orange diamonds.

are in agreement with other literature on LHCEs: Bergstrom *et al.* and Sudoh *et al.* reported negative values for like-ion correlations and positive values for unlike-ion correlations, too, for DMC and sulfolane based LHCEs, respectively.[14,52]

A more detailed comparison of the LiTFSI-based system on the left-hand side and the LiFSI-based system in the middle section shows that the ion correlations in the FSI-based system increase slightly stronger compared to the TFSI-based system. Thus, the anion structure has an impact on the ion dynamics: As discussed above, the lower interfacial activity of FSI^- results in more pronounced Li–anion networks with a large share of strong bidentate Li–anion coordination leading to the stronger increase in ion–ion correlations compared to the LiTFSI(1.8) system. Thus, even if the effect is small, the dynamics of the conducting salt phase as a function of the degree of dilution depend on the anion structure. A less surface-active anion leads to a more compact conducting salt phase with a coherent flux, while the like-ion anticorrelations remain stronger in a system with a more surface-active anion and a fuzzier and softer conducting salt phase.

The most significant increase is found for the highly concentrated LiFSI(1.2) system in the right panel of Fig. 7 (note the different scaling of the y axis). Here, the two like-ion correlations also become positive with the addition of TTE. Thus, the conducting salt concentration has a strong influence on the ion correlations: Due to the discussed structural properties of a strong bridging of anions between Li^+ and a large conducting salt phase with minimized interface to the diluent phase, a pronounced coherent motion of the conducting salt phase is expected and can explain the observed strongly positive values for the Onsager coefficients.

CONCLUSIONS

LHCEs are characterized by their complex microstructure of two immiscible phases, the conducting salt phase and the diluent phase. In this study, we perform MD simulations to elucidate not only the lithium coordination in the conducting salt phase but also the size and composition of its interface toward the diluent phase in dependence on the anion structure, conducting salt concentration, and degree of dilution. We find that the molecular structure of the anion largely impacts both, size and composition of the interface, which in turn influences the dynamics in the systems.

On the one hand, $TFSI^-$ anions are, in comparison with FSI^- anions, larger and more amphiphilic due to the increased charge delocalization. Therefore, the packing in the conducting salt phase is less efficient, resulting in smaller Li–anion coordination numbers and Li–anion networks in comparison with the LiFSI-based systems. Furthermore, due to the amphiphilic character, $TFSI^-$ anions are surface-active toward the diluent phase. They interact with the diluent molecules at the internal interface, which leads to a beneficial formation and an enrichment of anions at the conducting salt|diluent interface resulting in increased ion dissociation.

In terms of dynamics, we show that the structural features (enrichment of the anion at the internal interface, resulting in smaller Li–anion networks) in the TFSI-based LHCE lead to the smallest increase in ion correlations upon dilution. In general, the ion correlations increase with the addition of diluent since the diluent phase compensates coherent flux of the conducting salt phase. However, this effect is comparatively small in the LiTFSI-based LHCE since the cation–anion networks in the conducting salt phase are rather small and the interface toward the diluent phase large and fuzzy. Thus, we do not observe a pronounced coherent motion of the conducting salt phase and especially the motion of like-ions is still anti-correlated.

On the other hand, FSI^- anions are smaller and have a more localized charge distribution. Compared to the LiTFSI-based system, we find a higher lithium coordination number especially for bidentate coordination and larger Li–anion networks due to a more efficient packing of the conducting salt phase. This difference compared to the LiTFSI-based system is even more pronounced in the higher concentrated LiFSI(1.2) system. Here, one large Li–anion network percolates the entire simulation box, and due to the high conducting salt concentration, the anions connect not only two cations linearly, as in the other LHCEs, but also bind up to four Li^+ in a branched manner.

As FSI^- anions are less amphiphilic, we also do not observe a preferred interaction with diluent molecules, unlike $TFSI^-$ anions. In the case of the LiFSI(1.8) system, this leads to a statistical distribution of anions and solvent molecules at the internal interface, and in the higher concentrated LiFSI(1.2) system, we even observe a solvent-enriched interface, as described by Efaw *et al.* for a LiFSI–DME–TFEO LHCE.[16] Due to the large and branched Li–anion network in the latter, the formation of the conducting salt|diluent interface is so unfavorable that its size remains largely unchanged upon dilution and does not increase as in the other systems.

Furthermore, the larger size of the Li–anion networks (compared to the TFSI-based system) leads to a stronger coherent motion of the conducting salt phase and hence to more pronounced positive ion correlations. While the like-ion correlations remain negative in the LiFSI(1.8) system similar to the LiTFSI-based LHCE, we only observe positive correlation (unlike-ion and like-ion) in the highly concentrated LiFSI(1.2) system. The branched Li–anion network and minimized interface toward the diluent phase lead to a strong coherent movement of the conducting salt phase compensated by a diluent phase flux.

In conclusion, we show that the size and composition of the internal interface in LHCEs depend on the anion structure and conducting salt concentration. Conversely, this also affects the composition in the core of the conducting salt phase and, hence, the lithium coordination and transport. Therefore, it is a crucial element of LHCEs, which can be easily investigated by the presented evaluation based on the Voronoi analysis implemented in the software Travis. A deepened knowledge on the internal interface can help design LHCEs consisting of components that improve the interface formation and hence enhance transport properties.

Future studies might focus on how far these observations persist near electrode interfaces. In this context, it would also be intriguing to study how the transport properties change under strong electric fields. While we expect that mainly the constituents of the conducting salt phase would form the electrical double layer and that the Li^+ desolvation kinetics is rather similar to the corresponding HCE, MD simulations with explicit interfaces could provide valuable insights, possibly in combination with quantum chemical calculations to rationalize the electrochemical stability of LHCEs.

SUPPLEMENTARY MATERIAL

See the supplementary material for MD simulation details (number of molecules, box volume), densities (MD and experimental), self-diffusion coefficients (MD and experimental), radial distribution functions, lithium coordination numbers, Li–anion network, equations for discussed quantities, and ionicities (MD and experimental).

ACKNOWLEDGMENTS

A.H. was supported by the Ministry of Culture and Science of the State North Rhine Westphalia in course of the International Graduate School for Battery Chemistry, Characterization, Analysis, Recycling and Application (BACCARA). The MD simulations for this work were performed on the computer cluster PALMA II of the University of Münster.

AUTHOR DECLARATIONS

Conflict of Interest

The authors have no conflicts to disclose.

Author Contributions

Anne Hockmann: Conceptualization (lead); Data curation (equal); Formal analysis (lead); Funding acquisition (equal); Investigation (lead); Methodology (lead); Project administration (equal); Software (equal); Validation (lead); Visualization (lead); Writing – original draft (lead); Writing – review & editing (equal). **Monika Schönhoff**: Funding acquisition (equal); Project administration (equal); Resources (equal); Supervision (equal); Writing – review & editing (equal). **Diddo Diddens**: Data curation (equal); Resources (equal); Software (equal); Supervision (equal); Writing – review & editing (equal).

DATA AVAILABILITY

The data that support the findings of this study are available from the corresponding author upon reasonable request.

REFERENCES

[1] E. J. Berg, C. Villevieille, D. Streich, S. Trabesinger, and P. Novák, "Rechargeable batteries: Grasping for the limits of chemistry," J. Electrochem. Soc. **162**(14), A2468–A2475 (2015).

[2] Q. Wang, B. Liu, Y. Shen, J. Wu, Z. Zhao, C. Zhong, and W. Hu, "Confronting the challenges in lithium anodes for lithium metal batteries," Adv. Sci. **8**(17), e2101111 (2021).

[3] X. Cao, H. Jia, W. Xu, and J.-G. Zhang, "Review—Localized high-concentration electrolytes for lithium batteries," J. Electrochem. Soc. **168**(1), 010522 (2021).

[4] Y. Yamada, J. Wang, S. Ko, E. Watanabe, and A. Yamada, "Advances and issues in developing salt-concentrated battery electrolytes," Nat. Energy **4**(4), 269–280 (2019).

[5] J. Hu, Y. Ji, G. Zheng, W. Huang, Y. Lin, L. Yang, and F. Pan, "Influence of electrolyte structural evolution on battery applications: Cationic aggregation from dilute to high concentration," Aggregate **3**(1), e153 (2022).

[6] J. Qian, W. A. Henderson, W. Xu, P. Bhattacharya, M. Engelhard, O. Borodin, and J. G. Zhang, "High rate and stable cycling of lithium metal anode," Nat. Commun. **6**, 6362 (2015).

[7] S. Chen, J. Zheng, D. Mei, K. S. Han, M. H. Engelhard, W. Zhao, W. Xu, J. Liu, and J. G. Zhang, "High-voltage lithium-metal batteries enabled by localized high-concentration electrolytes," Adv. Mater. **30**(21), e1706102 (2018).

[8] X. Ren, P. Gao, L. Zou, S. Jiao, X. Cao, X. Zhang, H. Jia, M. H. Engelhard, B. E. Matthews, H. Wu, H. Lee, C. Niu, C. Wang, B. W. Arey, J. Xiao, J. Liu, J. G. Zhang, and W. Xu, "Role of inner solvation sheath within salt–solvent complexes in tailoring electrode/electrolyte interphases for lithium metal batteries," Proc. Natl. Acad. Sci. U. S. A. **117**(46), 28603–28613 (2020).

[9] K. Dokko, N. Tachikawa, K. Yamauchi, M. Tsuchiya, A. Yamazaki, E. Takashima, J.-W. Park, K. Ueno, S. Seki, N. Serizawa, and M. Watanabe, "Solvate ionic liquid electrolyte for Li–S batteries," J. Electrochem. Soc. **160**(8), A1304–A1310 (2013).

[10] X. Ren, L. Zou, X. Cao, M. H. Engelhard, W. Liu, S. D. Burton, H. Lee, C. Niu, B. E. Matthews, Z. Zhu, C. Wang, B. W. Arey, J. Xiao, J. Liu, J.-G. Zhang, and W. Xu, "Enabling high-voltage lithium-metal batteries under practical conditions," Joule **3**(7), 1662–1676 (2019).

[11] H. Jia, Y. Xu, X. Zhang, S. D. Burton, P. Gao, B. E. Matthews, M. H. Engelhard, K. S. Han, L. Zhong, C. Wang, and W. Xu, "Advanced low-flammable electrolytes for stable operation of high-voltage lithium-ion batteries," Angew. Chem., Int. Ed. **60**(23), 12999–13006 (2021).

[12] X. Chen and H. Yu, "A computational review on localized high-concentration electrolytes in lithium batteries," ChemElectroChem **11**(23), e202400444 (2024).

[13] Y. Wu, A. Wang, Q. Hu, H. Liang, H. Xu, L. Wang, and X. He, "Significance of antisolvents on solvation structures enhancing interfacial chemistry in localized high-concentration electrolytes," ACS Cent. Sci. **8**(9), 1290–1298 (2022).

[14] H. K. Bergstrom and B. D. McCloskey, "Ion transport in (localized) high concentration electrolytes for Li-based batteries," ACS Energy Lett. **9**(2), 373–380 (2024).

[15] Y. Watanabe, Y. Ugata, K. Ueno, M. Watanabe, and K. Dokko, "Does Li-ion transport occur rapidly in localized high-concentration electrolytes?," Phys. Chem. Chem. Phys. **25**(4), 3092–3099 (2023).

[16] C. M. Efaw, Q. Wu, N. Gao, Y. Zhang, H. Zhu, K. Gering, M. F. Hurley, H. Xiong, E. Hu, X. Cao, W. Xu, J. G. Zhang, E. J. Dufek, J. Xiao, X. Q. Yang, J. Liu, Y. Qi, and B. Li, "Localized high-concentration electrolytes get more localized through micelle-like structures," Nat. Mater. **22**(12), 1531–1539 (2023).

[17] A. Hockmann, P. Yan, D. Diddens, I. Cekic-Laskovic, and M. Schönhoff, "Impact of the anion structure on coordination and dynamics in a localized high-concentration battery electrolyte," J. Phys. Chem. B **129**(25), 6289–6299 (2025).

[18] M. Brehm, H. Weber, M. Thomas, O. Hollóczki, and B. Kirchner, "Domain analysis in nanostructured liquids: A post-molecular dynamics study at the example of ionic liquids," ChemPhysChem **16**(15), 3271–3277 (2015).

[19] M. Brehm and B. Kirchner, "TRAVIS–A free analyzer and visualizer for Monte Carlo and molecular dynamics trajectories," J. Chem. Inf. Model. **51**(8), 2007–2023 (2011).

[20] M. Brehm, M. Thomas, S. Gehrke, and B. Kirchner, "TRAVIS—A free analyzer for trajectories from molecular simulation," J. Chem. Phys. **152**(16), 164105 (2020).

[21] M. J. Abraham, T. Murtola, R. Schulz, S. Páll, J. C. Smith, B. Hess, and E. Lindahl, "GROMACS: High performance molecular simulations through multi-level parallelism from laptops to supercomputers," SoftwareX **1–2**, 19–25 (2015).

[22] J. N. Canongia Lopes and A. A. H. Pádua, "CL&P: A generic and systematic force field for ionic liquids modeling," Theor. Chem. Acc. **131**(3), 1129 (2012).

[23] W. L. Jorgensen, D. S. Maxwell, and J. Tirado-Rives, "Development and testing of the OPLS all-atom force field on conformational energetics and properties of organic liquids," J. Am. Chem. Soc. **118**(45), 11225–11236 (1996).

[24] L. S. Dodda, I. Cabeza de Vaca, J. Tirado-Rives, and W. L. Jorgensen, "LigParGen web server: An automatic OPLS-AA parameter generator for organic ligands," Nucleic Acids Res. **45**(W1), W331–W336 (2017).

[25]N. Molinari, J. P. Mailoa, and B. Kozinsky, "Effect of salt concentration on ion clustering and transport in polymer solid electrolytes: A molecular dynamics study of PEO–LiTFSI," Chem. Mater. **30**(18), 6298–6306 (2018).
[26]A. Thum, A. Heuer, K. Shimizu, and J. N. Canongia Lopes, "Solvate ionic liquids based on lithium bis(trifluoromethanesulfonyl)imide–glyme systems: Coordination in MD simulations with scaled charges," Phys. Chem. Chem. Phys. **22**(2), 525–535 (2020).
[27]L. Martínez, R. Andrade, E. G. Birgin, and J. M. Martínez, "PACKMOL: A package for building initial configurations for molecular dynamics simulations," J. Comput. Chem. **30**(13), 2157–2164 (2009).
[28]N. Michaud-Agrawal, E. J. Denning, T. B. Woolf, and O. Beckstein, "MDAnalysis: A toolkit for the analysis of molecular dynamics simulations," J. Comput. Chem. **32**(10), 2319–2327 (2011).
[29]R. J. Gowers, M. Linke, J. Barnoud, T. J. E. Reddy, M. N. Melo, S. L. Seyler, J. Domanski, D. L. Dotson, S. Buchoux, I. M. Kenney, and O. Beckstein, "MDAnalysis: A Python package for the rapid analysis of molecular dynamics simulation," in *Proceedings of the Python in Science Conference* (SciPy Consortium, 2016), pp. 98–105.
[30]X. Cao, P. Gao, X. Ren, L. Zou, M. H. Engelhard, B. E. Matthews, J. Hu, C. Niu, D. Liu, B. W. Arey, C. Wang, J. Xiao, J. Liu, W. Xu, and J. G. Zhang, "Effects of fluorinated solvents on electrolyte solvation structures and electrode/electrolyte interphases for lithium metal batteries," Proc. Natl. Acad. Sci. U. S. A. **118**(9), e2020357118 (2021).
[31]G. Zhang, J. Chang, L. Wang, J. Li, C. Wang, R. Wang, G. Shi, K. Yu, W. Huang, H. Zheng, T. Wu, Y. Deng, and J. Lu, "A monofluoride ether-based electrolyte solution for fast-charging and low-temperature non-aqueous lithium metal batteries," Nat. Commun. **14**(1), 1081 (2023).
[32]S. Perez Beltran, X. Cao, J.-G. Zhang, and P. B. Balbuena, "Localized high concentration electrolytes for high voltage lithium–metal batteries: Correlation between the electrolyte composition and its reductive/oxidative stability," Chem. Mater. **32**(14), 5973–5984 (2020).
[33]A. Hockmann, F. Ackermann, D. Diddens, I. Cekic-Laskovic, and M. Schönhoff, "Heterogeneous Li coordination in solvent-in-salt electrolytes enables high Li transference numbers," Faraday Discuss. **253**, 343–364 (2024).
[34]M. Bochenska, V. C. Kravtsov, and V. E. Zavodnik, "X-ray structure and proton NMR study of a hexacoordinated lithium complex," J. Inclusion Phenom. Mol. Recognit. Chem. **28**(2), 125–140 (1997).
[35]X. Bogle, R. Vazquez, S. Greenbaum, A. v. W. Cresce, and K. Xu, "Understanding Li^+–solvent interaction in nonaqueous carbonate electrolytes with ^{17}O NMR," J. Phys. Chem. Lett. **4**(10), 1664–1668 (2013).
[36]W. A. Henderson, N. R. Brooks, W. W. Brennessel, and V. G. Young, "Triglyme–Li^+ cation solvate structures: Models for amorphous concentrated liquid and polymer electrolytes (I)," Chem. Mater. **15**(24), 4679–4684 (2003).
[37]K. Yuan, H. Bian, Y. Shen, B. Jiang, J. Li, Y. Zhang, H. Chen, and J. Zheng, "Coordination number of Li^+ in nonaqueous electrolyte solutions determined by molecular rotational measurements," J. Phys. Chem. B **118**(13), 3689–3695 (2014).
[38]U. Olsher, R. M. Izatt, J. S. Bradshaw, and N. K. Dalley, "Coordination chemistry of lithium ion: A crystal and molecular structure review," Chem. Rev. **91**(2), 137–164 (1991).
[39]G. Mao, M.-L. Saboungi, D. L. Price, M. B. Armand, and W. S. Howells, "Structure of liquid PEO-LiTFSI electrolyte," Phys. Rev. Lett. **84**(24), 5536–5539 (2000).
[40]L. T. Costa, B. Sun, F. Jeschull, and D. Brandell, "Polymer-ionic liquid ternary systems for Li-battery electrolytes: Molecular dynamics studies of LiTFSI in a EMIm-TFSI and PEO blend," J. Chem. Phys. **143**(2), 024904 (2015).
[41]A. Thum, D. Diddens, and A. Heuer, "Impact of charged surfaces on the structure and dynamics of polymer electrolytes: Insights from atomistic simulations," J. Phys. Chem. C **125**(46), 25392–25403 (2021).
[42]Z. Li, G. D. Smith, and D. Bedrov, "Li^+ solvation and transport properties in ionic liquid/lithium salt mixtures: A molecular dynamics simulation study," J. Phys. Chem. B **116**(42), 12801–12809 (2012).
[43]D. Rakov, M. Hasanpoor, A. Baskin, J. W. Lawson, F. Chen, P. V. Cherepanov, A. N. Simonov, P. C. Howlett, and M. Forsyth, "Stable and efficient lithium metal anode cycling through understanding the effects of electrolyte composition and electrode preconditioning," Chem. Mater. **34**(1), 165–177 (2021).
[44]L. Su, F. Lu, X. Liu, C. Wang, Y. Gao, S. Passerini, L. Zheng, and G. Xinpei, "Molecular insight into nano-heterogeneity of localized high-concentration electrolyte: Correlation with lithium dynamics and solid-electrolyte interphase formation," J. Power Sources **557**, 232545 (2023).
[45]W. van Ekeren, A. Hall, K. Lahtinen, and R. Younesi, "The solvation structure of localized high concentration electrolytes," ChemElectroChem **11**(11), e202400050 (2024).
[46]Y. Zeng, S. Zhang, Y. Yao, J. Liu, N. Zhou, J. Tang, K. Zhang, Y. Li, J. Hu, B. Yang, C. Peng, and H. Liu, "Structure and interaction of ionic liquid monolayer on lithium from first-principles," J. Phys. Chem. C **128**(39), 16766–16780 (2024).
[47]D. Bedrov, J. P. Piquemal, O. Borodin, A. D. MacKerell, Jr., B. Roux, and C. Schröder, "Molecular dynamics simulations of ionic liquids and electrolytes using polarizable force fields," Chem. Rev. **119**(13), 7940–7995 (2019).
[48]H. Kilian, T. Pothmann, M. Lorenz, M. Middendorf, S. Seus, M. Schönhoff, and B. Roling, "Quantification of vehicular versus uncorrelated Li^+–solvent transport in highly concentrated electrolytes via solvent-related Onsager coefficients," Phys. Chem. Chem. Phys. **27**(3), 1593–1603 (2025).
[49]T. Pothmann, M. Middendorf, C. Gerken, P. Nürnberg, M. Schönhoff, and B. Roling, "Overdetermination method for accurate dynamic ion correlations in highly concentrated electrolytes," Faraday Discuss. **253**, 100–117 (2024).
[50]F. Kilchert, M. Lorenz, M. Schammer, P. Nürnberg, M. Schönhoff, A. Latz, and B. Horstmann, "A volume-based description of transport in incompressible liquid electrolytes and its application to ionic liquids," Phys. Chem. Chem. Phys. **25**(38), 25965–25978 (2023).
[51]D. Diddens and A. Heuer, "Hydrodynamic interactions in ion transport—Theory and simulation," J. Chem. Phys. **158**(15), 154112 (2023).
[52]T. Sudoh, S. Ikeda, K. Shigenobu, S. Tsuzuki, K. Dokko, M. Watanabe, W. Shinoda, and K. Ueno, "Li-ion transport and solution structure in sulfolane-based localized high-concentration electrolytes," J. Phys. Chem. C **127**(25), 12295–12303 (2023).